Solid-State Emission from Mono- and Bichromophoric Boron Dipyrromethene (BODIPY) Derivatives and Comparison with Fluid Solution

Özgür Altan Bozdemir,[a,b] Hatun H. T. Al-Sharif,[a] William McFarlane,[c] Paul G. Waddell,[d] Andrew C. Benniston[a] and Anthony Harriman*[a]

Dedicated to Dr. Raymond Ziessel in recognition of his seminal contributions to this subject

Abstract: The syntheses and crystal structures of sterically-crowded mono- and bichromophoric BODIPY-based dyes are reported. The "monomeric" compound is weakly fluorescent in the liquid phase due to fast internal conversion associated with rotation of aryl rings at the boron atom. The side-by-side "dimer" exhibits weak excitonic coupling between the dipyrrin units and is much more emissive in fluid solution. Solid samples of both compounds are strongly fluorescent under near-UV illumination. Thus, the mono-chromophore exhibits dual fluorescence from what appears to be a mixture of crystalline and possibly amorphous (or interfacial regions) distributions. The bi-chromophore packs in the crystal as pairs of chromophores with each unit being provided by a different molecule. This leads to excitonic splitting and the formation of a strong H-band in the absorption spectrum. Fluorescence occurs from the corresponding J-species and also from what appears to be an aggregated state associated with interfacial areas. Both bulk and interface-bound states show relatively long-lived fluorescence while the crystal structures indicate the likelihood for fast electronic energy migration between molecules.

Introduction

The boron dipyrromethene (BODIPY) family of fluorescent dyes has undergone extensive expansion and diversification over the past decade or so.[1-4] These compounds now rival cyanine dyes[5] for their versatility and scope and have found numerous applications as fluorescent labels and sensors.[6,7] Indeed, BODIPY dyes are widely recognized as being robust and photostable but perhaps their most significant advantage stems from the facile structural modification inherent to the dipyrrin core. Conventional organic coupling strategies allow substitution of an almost limitless variety of ancillary groups at the various carbon atoms and this has led to a vast treasure trove of functional molecules. Incorporating heteroatoms into the dipyrrin framework[8,9] has allowed further manipulation of the optical properties. A major advance in this area was achieved by the introduction of synthetic protocols[10] to replace the usual B-F groups with B-C or B-O analogues. This promotes electronic isolation of the appended subunits and alters the molecular topology, taking advantage of the tetrahedral geometry at the boron atom. Certain such derivatives are active in terms of circularly polarized luminescence.[11]

Nowadays, there is growing interest in the development of photonic crystals[12] and several BODIPY derivatives have been reported to fluoresce when in the crystalline phase.[13] Such behaviour is unusual since proximal molecular interactions tend to promote radiationless decay of excited singlet states. This latter situation is a serious problem for the design of artificial light-harvesting antennae since high absorption cross-sections are needed[14] but individual molecules must be isolated in electronic terms. Natural photosynthetic antennae overcome this dichotomy by careful positioning of the chromophores on a protein scaffold.[15] The same general type of highly ordered arrays of chromophores should be possible with certain crystals if π,π interactions can be controlled without compromising the high absorptivity of the condensed solid. Thus, the question arises as to whether emissive crystals might be engineered using BODIPY derivatives with steric blocking units attached at the boron atom.

Here, we examine the feasibility of blocking close association of the BODIPY fluorophores using phenyl groups in place of the conventional fluorine atoms. Specifically, we describe the synthesis of ethylene-bridged *meso*-aryl-C-BODIPY through the reaction of a *meso*-aryl-F-BODIPY with aryllithium reagents. Although the synthetic strategy is known, no detailed photophysical study has been reported for such compounds and there are no known fluorescent crystalline B-aryl derivatives. Apart from manipulating crystal packing, the geometry around the boron atom contributes to the molecular structure of side-by-side BODIPY-based bichromophores.[16,17] Again, this is a rich field in its own right and there are several descriptions of excitonic coupling in BODIPY-based bichromophores and higher analogues.[18] Slight modification of the synthetic strategy used here allows isolation of the corresponding bichromophores with an ethylene linkage between the two dipyrrin units.

[a] Prof. Dr. OA Bozdemir, HHT Al-Sharif, Prof. Dr. AC Benniston, Prof. Dr. A Harriman
Molecular Photonics Laboratory, School of Natural and Environmental Science (SNES)
Newcastle University, Newcastle upon Tyne, NE1 7RU, UK
E-mail: anthony.harriman@ncl.ac.uk
[b] Prof. Dr. OA Bozdemir
Department of Chemistry, Ataturk University, Erzurum, 25240, Turkey.
[c] Prof. W McFarlane
NMR Laboratory, SNES, Newcastle University, Newcastle upon Tyne, NE1 7RU, UK
[d] Dr.PG Waddell
Crystallography Laboratory, SNES, Newcastle University, Newcastle upon Tyne, NE1 7RU, UK

Supporting information for this article is given via a link at the end of the document.

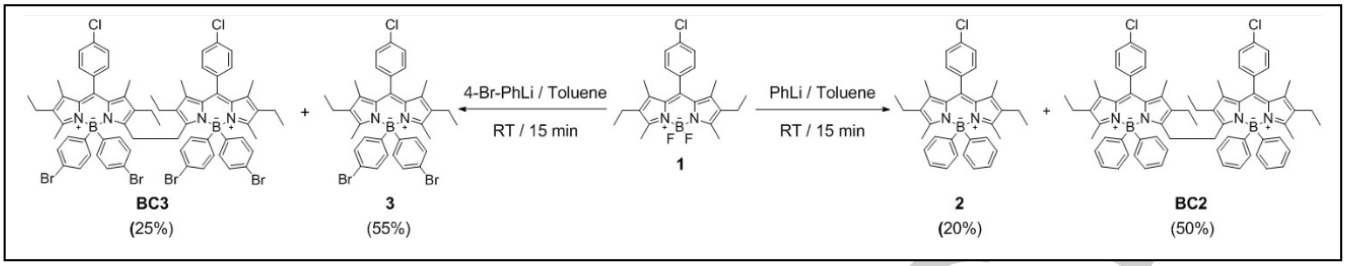

Scheme 1. Outline of the generic synthetic strategy adopted for the preparation of the main target compounds investigated here.

Results and Discussion

Synthesis and characterization

In recent years, metal-catalyzed coupling reactions,[19] nucleophilic aromatic substitutions,[20] and reactions with organo-metallic reagents[21] have been applied to synthesize novel BODIPY derivatives. In addition to the boron difluoride complexes (4,4-difluoro-4-bora-3a,4a-diaza-s-indacene; F-BODIPY), a plethora of new dialkyl- or diaryl- (C-BODIPY), dialkynyl- (E-BODIPY), and dialkyloxy- or diaryloxy (O-BODIPY) derivatives have been isolated *via* the "substitution at boron approach" pioneered by Ziessel.[10] These reactions are made possible using the corresponding Grignard reagents, alkyl- or aryllithium salts, and alkyl- or aryloxy-base. In particular, certain E-BODIPY derivatives, featuring comparable photophysical properties to the parent F-BODIPY, have been exploited as energy donating and/or accepting modules in cassette- or cascade-type light-harvesting systems.[22,23]

In the course of our attempts to modify *meso*-aryl-F-BODIPY dyes at the boron centre, we first studied the reaction of 8-(4-chlorophenyl)-BODIPY, **1**, with phenyllithium in anhydrous toluene at room temperature (Scheme 1). This reaction, unlike the literature methods developed for the aryl-fluoride substitution reactions of 8-methyl-and 8-H-BODIPY derivatives,[24] did not proceed cleanly to give the expected product, **2**, in good yield; surprisingly, the reaction resulted in the formation of an ethylene-bridged bichromophore, **BC-2**, *via* reaction of the strongly basic phenyl anion with one of the methyl groups of the starting BODIPY or diphenyl-substituted **2** present in the reaction medium.

The ethylene-bridged F-BODIPY bichromophores and the corresponding oligomers have recently been synthesized[24] by reaction of F-BODIPY with ICl in the presence of lithium diisopropylamide (LDA) as a strong base to deprotonate the α-methyl groups. The nature of the BODIPY *meso*-appendage is not expected to have a significant effect on the dimerization process when the LDA/ICl system is used at -78 ºC. However, dimerization reactions carried out in the presence of aryllithium salts seem to depend critically on the type of *meso*-substituent.[25] In particular, there are no literature reports indicating that 8-H or 8-methyl BODIPY derivatives form bichromophores or oligomers during fluorine replacement with an aryllithium.

It is clear that the 8-aryl group in **1** drastically changes the reactivity of this compound and causes an alkyl-alkyl coupling not previously observed for 8-methyl- or 8-H-BODIPY derivatives. Notably, when freshly prepared 4-bromophenyllithium in dry toluene was used, the same type of dimerization took place to yield the corresponding ethylene-bridged bichromophore, **BC3**, in excellent yield, proving the generality of this reaction (Scheme 1). It should be noted that, in contrast to the dimerization/oligomerization protocol using the LDA/ICl procedure, higher oligomers were not detected in an intractable mixture of polar decomposition products. The methodology introduced here, therefore, is suitable for the selective generation of bichromophores. It will be noted that these latter compounds are highly substituted around the dipyrrin nucleus.

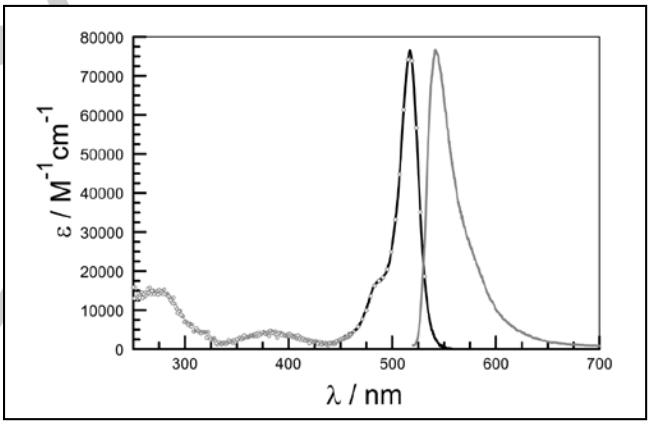

Figure 1. Normalized absorption (black curve), fluorescence (grey curve) and excitation (open circles) spectra recorded for **2** in CH_2Cl_2 solution at room temperature.

Photophysical properties in fluid media

The target mono-chromophoric compound, **2**, in fluid solution shows a pronounced absorption transition in the 450-550 nm region with a maximum (λ_{MAX}) at ca. 517 nm (Figure 1). The molar absorption coefficient at the band maximum (ε_{MAX}) is 76,640 M^{-1} cm^{-1}, corresponding to an oscillator strength of 0.39 for the lowest-energy absorption transition. This absorption profile can be deconstructed into a small series of Gaussian-shaped components, corresponding to vibronic satellites with a spacing of 650 cm^{-1}. The half-width for each Gaussian component is *ca*. 705 cm^{-1} (Figure S0). Changing the polarity of the solvent has only marginal effects on the position or shape of the absorption band.

Fluorescence can be observed for **2** in fluid solution, the emission maximum (λ_{FLU}) appearing at 543 nm (Figure 1). The corresponding Stokes shift is 920 cm^{-1}. Again, the emission profile can be deconstructed into a series of vibronic satellites with an average spacing of 520 cm^{-1} and a band half-width of 565 cm^{-1} (Figure S0).The Huang-Rhys factor[26] (S) for the fluorescence band has a value of 0.59, which is rather high for a pure π,π^* transition.[27] The choice of solvent has no obvious effect on the emission profile or the deconstruction pattern. From the Gaussian band shape analysis, the Stokes shift can be refined as being 835 cm^{-1}. The photophysical properties recorded in dilute solution are collected in Table 1, together with those obtained for **3**.

For **2** in pentan-1-ol solution, the fluorescence quantum yield (Φ_F) is 0.030 ± 0.005. A similar value was recorded in dioxane, tetrahydrofuran and CH_2Cl_2. The excited-singlet state lifetime (τ_S), measured by time-correlated, single photon counting, was found to be 0.36 ± 0.08 ns, with a minor (i.e., <3%) contribution of a longer-lived (i.e., 3.5 ns) species assigned to a trace impurity. Both Φ_F and τ_S are very low compared to the conventional BODIPY dye with BF_2 in place of the B-aryl groups.[28] The radiative rate constant ($k_{RAD} = \Phi_F/\tau_S = 1 \times 10^8\ s^{-1}$) is in good agreement with that ($k_{SB} = 1.3 \times 10^8\ s^{-1}$) calculated from the Strickler-Berg expression.[29] Of the literature reports referring to fluorescence from related B-aryl BODIPY fluorophores, two describe strong emission in fluid solution[25,30] but a third details weak emission at room temperature.[31] This latter report mentions that emission is recovered in a frozen glass at 77K.

Loss of fluorescence for **2** is clearly a consequence of the aryl rings appended to the boron centre; the same is true for **3** (Table 1). The absence of a polarity effect suggests that intramolecular charge transfer is not responsible for fluorescence quenching.[31] There is, however, a small recovery of emission on increasing the viscosity of the solvent (Figure S0). This can be done conveniently by using a series of linear alcohol solvents at fixed temperature. There is a steady increase in both Φ_F and τ_S with increasing viscosity but the effect is small. Molecular dynamics simulations indicate that the *meso*-aryl ring cannot rotate around the connecting C-C bond, but it can gyrate around the mean dihedral angle of *ca*. 90^0. Similar simulations (*vide infra*) are consistent with the B-aryl rings undergoing rotation. This internal twisting is likely responsible for the modest viscosity effect observed here.

Dispersing **2** in a sucrose octa-acetate glass[32] recovers much of the expected fluorescence. Now, τ_S increases to *ca*. 1.2 ns while Φ_F becomes 0.15 ± 0.02. These values are still low compared to the parent BF_2 emitter[28] but can be used to argue that dynamic structural distortion is the underlying reason for the poor emission in fluid solution.[33] The fluorescence yield is relatively insensitive to changes in temperature when the compound is embedded in the sugar. Over the temperature range 303 to 348K, there is a small decrease in the excited-state lifetime. Fitting the data to the Arrhenius equation allows estimation of the activation energy for radiationless decay as being ca. 5 kJ/mol (Figure S0). The pre-exponential factor is 2.7 x $10^9\ s^{-1}$. It is quite likely that the fluorophore resides in a cavity in the sugar matrix and thereby escapes the anticipated freezing of aryl ring rotation by the viscous environment. Indeed, in decan-1-ol solution there is a modest temperature dependence, with emission decreasing at higher temperatures (Figure S0). The corresponding kinetic data give a linear fit to the Arrhenius equation, with a pre-exponential factor of 8.5 x $10^{11}\ s^{-1}$ and an activation energy of 15.5 kJ/mol. The latter is similar to the activation energy for the viscosity of the solvent,[34] suggesting there is a modest structural barrier associated with distortion of the dipyrrin fragment.

As reported for a related compound by Gao *et al.*,[31] **2** is strongly fluorescent in an optical glass at 80K. Indeed, in 2-methyltetrahydrofuran (MTHF), which forms a hard glass below 100K,[35] the fluorescence yield depends markedly on temperature (Figure 2). At 80K, Φ_F approaches unity while τ_S has a value of 6.5 ± 0.1 ns. As the glass melts to form an amorphous phase between 100 and 137K, **2** loses emission gradually with increasing temperature. In fluid solution, the Φ_F falls rapidly as the temperature rises. These qualitative findings confirm that some type of structural distortion is responsible for the restricted emission seen in fluid solution at ambient temperature.[36,37]

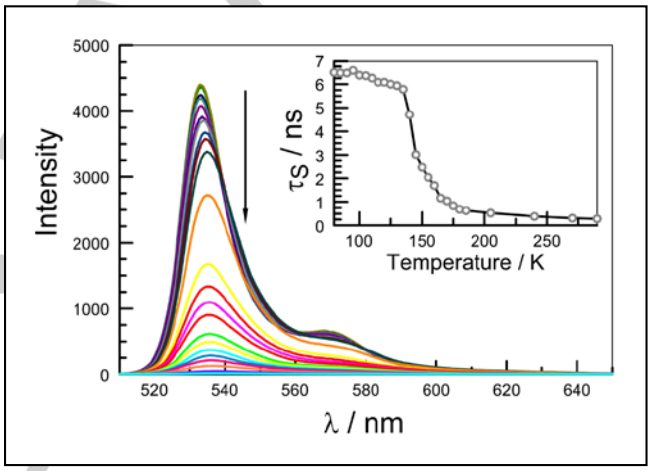

Figure 2. Effect of temperature on the fluorescence spectral profile recorded for **2** in MTHF. The arrow indicates the direction of increasing temperature from 80K to 290K. The insert shows how the fluorescence lifetime evolves with increasing temperature.

Radiationless deactivation of the first-excited singlet state of **2** is insignificant in the rigid glass formed at temperatures less than 100K. Under such conditions, Φ_F is ca. 0.95 and essentially independent of temperature. Nonradiative decay begins to compete with fluorescence throughout the amorphous phase and is weakly activated. Fluorescence remains the dominant process, however, across this region. Once the solvent melts (T_M = 137K),[35,36] nonradiative decay begins to dominate the excited-state dynamics (Figure 2). The radiationless decay rate constant (k_{NR}) can be derived from the experimental data on the basis that k_{RAD} is insensitive to changes in temperature. Across the liquid phase, k_{NR} increases with increasing temperature but approaches a plateau at ambient temperature (Figure S0). Such behaviour is unusual but earlier work[38] has reported non-linear viscosity effects for dyes that undergo photochemical isomerisation. For **2**, the observed behaviour can be explained in terms of a model where the rotor is partially screened from frictional forces with the

surrounding solvent. At low viscosity, other factors contribute to the rotational barrier and the viscosity effect becomes hidden.

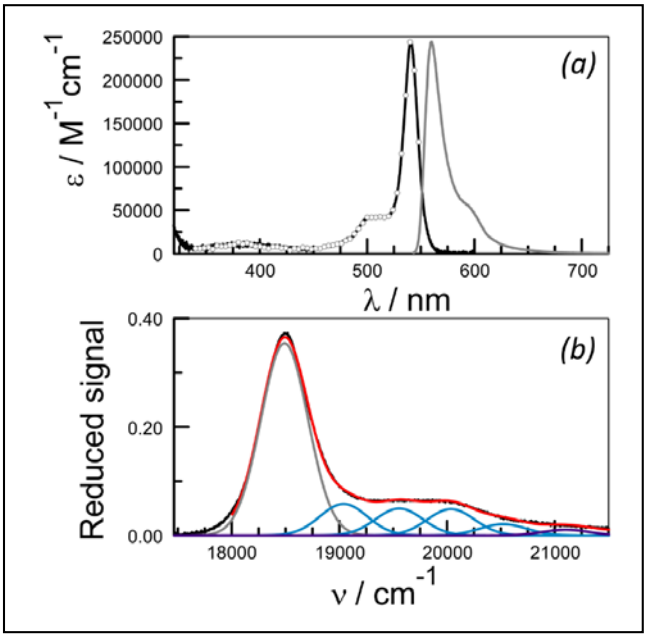

Figure 3. (a) Normalized absorption (black curve), fluorescence (grey curve) and excitation (open circles) spectra recorded for **BC2** in dilute CH_2Cl_2 solution at room temperature. (b) Example of a Gaussian deconstruction pattern obtained for the reduced absorption spectrum of **BC2** in CH_2Cl_2. The experimental spectrum is given in black and the reconstructed spectrum is shown in red. The individual Gaussian components are shown in grey (J- band) or blue (H-band).

The absorption spectrum recorded for the bichromophore **BC2** in CH_2Cl_2 solution exhibits a significant red shift relative to that measured for **2** (Figure 3a). The shift amounts to ca. 24 nm and there is an accompanying increase in the molar absorption coefficient at the band maximum (ε_{MAX} = 243,850 M^{-1} cm^{-1}). The latter exceeds twice the value recorded for **2** and is clear indication for some type of electronic interaction between the two chromophores for **BC2**. A similar effect was reported[24] earlier for somewhat related bichromophores and higher-order oligomers. Deconstruction of the absorption spectrum into Gaussian components (Figure 3b) does not give a similar progression to that described above for **2**. The half-width (FWHM = 515 cm^{-1}) is reduced, the 0,0 transition occurs at 18,490 cm^{-1} and there is no continuous progression of vibronic satellites. This situation is consistent with weak excitonic coupling between the two dipyrrin units.[39] In fact, analysis of the reduced spectrum indicates that the splitting between the two absorption transition dipoles is 520 cm^{-1}. Such excitonic coupling arises because the short connecting chain forces the respective transition dipole moment vectors into a crude alignment. A similar situation arises for **BC3**.

Molecular modelling (see Supporting Information) suggests a structure for **BC2** that has the two BODIPY units held in an oblique, in-line geometry with both boron atoms appearing on the same side of the molecule (Figure 4). The two chromophores are stepped by about 2Å and there are no obvious stacking events since the alkyl substituents and the B-aryl rings force the chromophores apart. The closest approach between the two dipyrrin units is 3.5Å while the centre-to-centre distance is *ca*. 8Å. Using the information derived from the computed structure in solution, the Kuhn extended dipole method[40] can be used to estimate the degree of excitonic coupling as being 130 cm^{-1}. This calculation, based entirely on dipole-dipole interactions, can be compared to the experimental value of 520 cm^{-1}. The Kasha model[41] for excitonic coupling between chromophores held in an oblique arrangement gives an estimate of the splitting energy of 255 cm^{-1} (see Supporting Information).

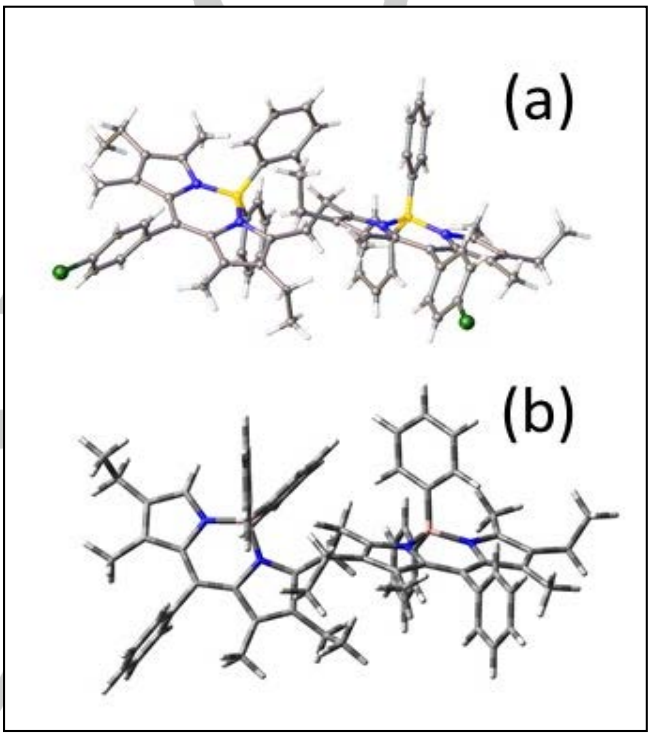

Figure 4. (a) Molecular structures obtained for the bichromophore **BC2** by X-ray crystallography. (b) Computed structure for an analogue of **BC2** lacking the chlorine atoms. The computation was made by DFT methods (PBE0/6-311G(d)/PCM($CHCl_3$) with Mennucci-Tomasi correction).

Fluorescence recorded for **BC2** in CH_2Cl_2 solution shows a red shift of 17 nm compared to **2**, with λ_{FLU} appearing at 560 nm (Figure 3a). Again, spectral deconstruction shows a progression of vibronic bands separated by *ca*. 380 cm^{-1}. The half-width (FWHM = 410 cm^{-1}) is decreased somewhat relative to that reported for the mono-chromophore, **2**, and there is a noticeable change in the Huang-Rhys factor for **BC2**. At room temperature in dilute solution, S decreases from 0.59 for **2** to 0.47 for **BC2**. In CH_2Cl_2, toluene and ethanol solutions solution, Φ_F measured for **BC2** is 0.30 ± 0.03 while τ_S is 2.5 ± 0.1 ns. These values are significantly higher than those recovered for **2** at ambient temperature and thereby indicate that most of the competing radiationless process is curtailed for the bichromophore (Table 1). At low temperature in an MTHF rigid glass, full recovery of the

Table 1. Compilation of the photophysical properties of the two target compounds measured at room temperature in fluid solution.

Compound	λ_{MAX} / nm	$\varepsilon_{MAX}/M^{-1}cm^{-1}$	λ_{FLU} / nm	Φ_F	τ_S / ns	k_{RAD} / 10^7 s^{-1}	SS / cm^{-1} [c]	S [d]	$h\omega_L$ / cm^{-1} [e]
2 [a]	517	76,640	543	0.027	0.36	10	835	0.59	520
BC2 [b]	541	243,850	560	0.30	2.5	12	610	0.48	380
3 [a]	519	74,780	544	0.019	0.18	11	865	0.55	495
BC3 [b]	541	214,300	557	0.27	2.35	11	690	0.47	400

[a] Dioxane solution. [b] CH_2Cl_2 solution.[c] Stokes shift. [d] Huang-Rhys factor. [e] Low-frequency vibronic mode coupled to deactivation of first singlet-excited state.

fluorescence (Φ_F = 0.97 ± 0.03) occurs. That moving from the "monomer" to the corresponding "dimer" switches off rapid radiationless decay of the emitting state is unusual and must have its origin in the molecular structure. Similar behaviour is found for **3** and **BC3**. Such an effect is most unexpected!

Structural studies for fluid media

Temperature-dependent ^{1}H NMR studies carried out with **2** in $CDCl_3$ solution show no obvious conformational exchange (Figure S0). Moreover, computational studies indicate that the *meso*-aryl ring cannot undergo full rotation around the connecting C-C bond (Figure S0). This situation is fully consistent with earlier studies made with conventional B-F BODIPY dyes.[1-4] Our results indicate a small energy barrier for rotation of the B-aryl rings in fluid solution (Figure S0); these calculations were made for analogues lacking the halogen atoms and therefore are applicable to both **2** and **3** (Figure 4). In order for one of the B-aryl rings to rotate by 180^0, it is necessary for the adjacent methyl groups to move out of the plane imposed by the dipyrrin unit and also for the second B-aryl ring to twist away from its mean position. The resultant rotational barrier is only ca. 10 kJ/mol for the ground state. During ring rotation, the lower rim of the dipyrrin unit in the vicinity of the boron atom becomes distorted. This structural modification is likely to introduce pinholes,[42] or conical intersections,[43]into the excited-state potential energy surface and thereby provide a new route for radiationless return to the ground state. It is this perturbation that causes loss of fluorescence from **2** in fluid solution. Such structural distortion will not occur in the rigid glass where the photophysical properties resemble those of the corresponding BF_2 complex.

The bichromophore, **BC2**, differs from **2** by virtue of an increased moment of inertia and by the introduction of electronic interaction between the two dipyrrin units. This latter effect is apparent from the lowered Huang-Rhys factor, S, which indicates increased electron delocalization for **BC2**.[26] The very high ε_{MAX} found for **BC2** also testifies to some type of electronic coupling between the two dipyrrin units.[44] The increased moment of inertia will dampen bending motions imposed on the dipyrrin units and this could be the origin of the somewhat decreased $h\omega_L$ (Table 1). However, none of these factors explain the significantly increased Φ_F and τ_S observed for **BC2** relative to **2** and confirmed *via* **3** and **BC3** (Table 1). To address this point, we return to NMR spectroscopy.

Liquid-phase NMR studies were performed using 500 and 700 MHz instruments, mainly on **3** and **BC3**, which give somewhat simpler spectra than **2** and **BC2**. The atom numbering schemes are displayed in Figures SX and SY, and complete assignments were made of the proton spectra of each compound and of the ^{13}C NMR spectrum of **2,** with the aid of COSY, NOESY, ROESY, HSQC and HMBC methodologies (see Supporting Information). Tables SX and SY summarize the main results. In addition, a partial assignment of the ^{13}C NMR spectrum of **BC3** at low temperature gave useful structural information. Measurements were undertaken in $CDCl_3$ and in CD_2Cl_2, but without significant differences.

Starting with **3**, it is to be anticipated that steric interactions between the protons of the chloro-phenyl ring and the adjacent methyl groups will lead to restricted rotation about the C_8–C_9 bond and to force sites 10 and 15 to be either above or below the main molecular "plane". This might be expected to bring about inequivalence of C_{11} and C_{15} and of H_{11} and H_{15}, However, for this to be observable it is necessary that the *potential* C_{2v} symmetry of the molecule is destroyed by an internal framework distortion, such as that found in the solid state (see below). In fact, in solution at temperatures down to 183K, sites 11 and 15 remain equivalent, and we conclude that in solution relevant distortions are averaged out on the NMR timescale. Similar considerations apply to the possible inequivalence of symmetry-related sites in the bromo-phenyl rings at the boron atoms, and, even at low temperature, 21 remains equivalent to 22, 26 and 27, as might be expected.

The situation is quite different for the bichromophore **BC3** where a number of putative symmetry-related sites are found to be inequivalent, especially at low temperature. In CD_2Cl_2 over the range 298–188K, the protons of the 4-chlorophenyl group display classic decoalescence behaviour, showing that at low temperature sites 10 and 14 are inequivalent, as are sites 11 and 13. This finding confirms that there must be a significant barrier to rotation about the C_8–C_9 bond and that the molecule as a whole lacks a plane of symmetry. This idea is supported by low temperature ^{13}C NMR spectra. For example, at 188K the rate of site interconversion is *ca.*15 s^{-1} compared with *ca.*40,000 s^{-1} at 298K. Note that these rates may well be determined by the process leading to a reduction in overall molecular symmetry rather than the barrier to rotation about the C_8–C_9 bond.

With **BC3**, the 4-bromophenyl rings appear to exhibit similar behaviour, but closer examination shows that, in fact, the process also involves the C-15 site exchanging with C-21. This implies

interchange of the environments of both 4-bromophenyl rings attached to the same boron atom. That this is observable again implies a reduction of the molecular symmetry. In principle, the foregoing does not demand that there is no restriction of rotation about the B–C_{15} and B–C_{21} bonds, but if this were significant then more complex spectra would be expected than are observed. The rates of site interconversion are about three times as fast as for the 4-chlorophenyl groups. It is likely that the fundamental process leading to the above observations will be restricted rotation about the 5a–5a' bond linking the two halves of the bi-chromophore. Line-shape simulations of the proton spectra for the chloro- and bromophenyl rings of **BC3** over the range 208 to 308K lead to linear Eyring plots (Figures S00). From these, Gibbs energies of activation are calculated to be 41.2 and 40.4 kJ mol^{-1}, respectively.

In solution at 298K, site interconversion is rapid and so the spectrum is relatively simple. In particular, the methylene protons of the bridge will be effectively equivalent, as is found. However, at 198K this rotation is seriously hindered, leading to a preferred conformation in which the bridging methylene protons 5a and 5a' constitute a relatively complex spin system which also interacts with other protons in the vicinity. Peripheral protons, such as 1-Me, 2a-Me, 3-Me, and 2a-CH_2, are relatively unaffected, whereas 5a-CH_2, 6a-CH_2 and 6a-Me are seriously perturbed. This is illustrated by the ROESY spectrum given in Figure 5 which indicates many strong interactions in this region.

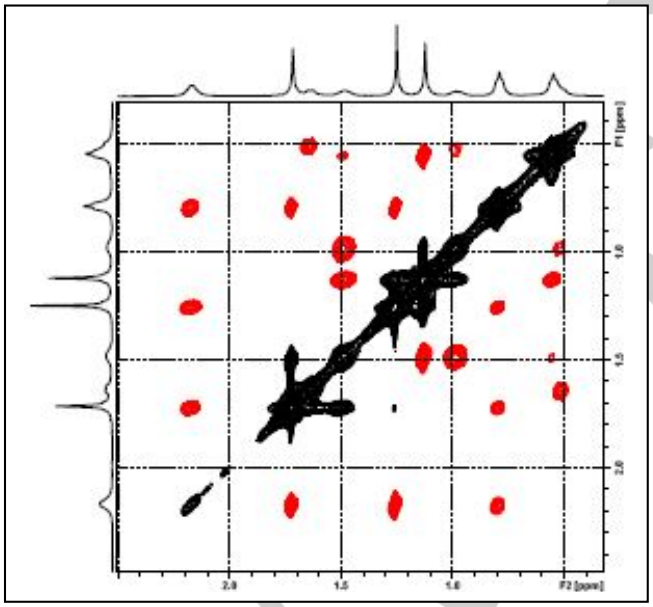

Figure 5. Part of the phase-sensitive 500 MHz proton 2D ROESY spectrum of **BC3** in CD_2Cl_2 at 195K with a mixing time of 250 ms. Negative off-diagonal peaks are shown in red and arise from n.O.e. interactions.

Although the NMR spectral data indicate substantial differences in rotational flexibility of the various aryl rings for the mono- and bichromophores, the origin of this effect remains obscure. It is likely that both steric and electronic terms contribute to the overall freezing of the rotations. The net result appears to be a reduction in access to pinholes in the excited-singlet state potential energy surface for the bichromophore in fluid solution. It seems likely that rotational freedom will be more restricted in the solid state and so attention now turns to crystalline samples of the target compounds.

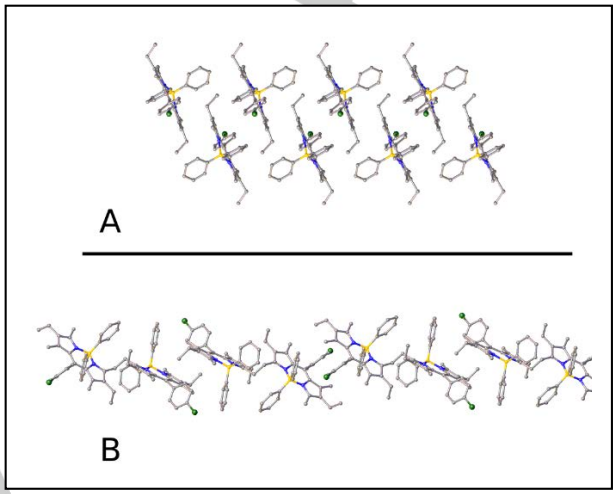

Figure 6. A view of the 'columns' formed of interactions involving the π-systems of the dipyrrin units in the crystal structures found for 2 (A) and BC2 (B).

X-Ray crystallography

The asymmetric unit of the crystal structure determined for **2** comprises two crystallographically independent molecules. In each of these arrangements, the boron atom is displaced from the dipyrrin unit, causing a loss of planarity (Figure 6a). The two B-aryl rings are displaced with respect to each other, resulting in a perturbed tetrahedral arrangement around the boron centre – this is not an unusual occurrence for BODIPY-based materials. In the supramolecular structure, **2** assembles into "columns" with adjacent units being co-facial, having a centre-to-centre distance of *ca*. 9.0 Å, but slightly offset and with the boron atoms lying on the same side of the molecule (Figure 6a). Such structures might be expected to facilitate long-range energy migration along the column in a random walk process.[45] It might be stressed here that electronic energy transfer between aligned dipoles can occur over 100 Å or more![46] Individual columns are isolated from their neighbours by voids, possibly created by repulsions between the chlorine atoms. These columns are almost mutually orthogonal with respect to the dipyrrin units and, therefore, are unlikely to promote inter-column electronic energy transfer. The situation for **3** remains somewhat similar (see Supporting Information).

The asymmetric unit of the crystal structure determined for **BC2** comprises half of the molecule and the two halves are related by a two-fold rotation about the centre of the C14-C14' bond. As a result, the two chromophores are crystallographically equivalent.and both boron atoms reside on the same side of the molecule, with a B···B separation of *ca*. 6.6 Å (Figure 4). The closest contact between the two dipyrrin units is *ca*. 3.4 Å and with a centre-to-centre distance of *ca*. 8.4 Å between the two planes.

The twist angle along the molecular axis is *ca*. 32^0 while the dihedral angle between the dipyrrin units is *ca*. 6^0. Each *meso*-aryl ring is subject to a dihedral angle of *ca.* 80^0 while the two C-B-C and N-B-N angles are $117.28(12)^0$ and $104.58(10)^0$, respectively. The molecular asymmetry imposed on the mono-chromophore is relaxed for the bichromophore, which appears to be symmetrical about the dipyrrin unit in the crystal.

The crystal packing observed for **BC2** is interesting in that the dipyrrin units align as co-facial pairs, held together by π···H interactions involving phenyl protons and the polarized pyrrin rings, with a modest offset (Figure 6b). The inter-chromophore separation is *ca*. 5.0 Å while the offset between the centres corresponds to *ca*. 4.0 Å . Each dipyrrin pair is related by inversion symmetry, which imposes long-range order. However, each pair of chromophores is separated from the next pair along the *pseudo*-chain by *ca*. 9.0 Å. Such a structure might be expected to localize the excitation energy within a molecular pair and for electronic energy transfer between pairs to be relatively ineffective. The chlorine atoms, together with the B-aryl rings, appear to play an important role in determining structural order and preventing close association between nearby units.

Photophysical properties for the solid state

It was observed that crystals of both **2** and **BC2** were strongly emissive when illuminated with a near-UV source. Such behaviour is uncommon since close molecular interactions usually serve to promote radiationless decay but there are literature examples of fluorescent BODIPY crystals.[13] However, emission from crystalline **2** and **BC2** appears to be strikingly bright, thereby meriting more detailed examination. These crystals did not degrade under prolonged illumination and could be embedded into plastic films formed by casting from solution.

The absorption spectrum recorded for single crystals of **2** exhibits a broad transition centred at around 522 nm which is reminiscent of that seen for **2** in dilute solution (Figure S0). There is also a weak, broad transition centred at ca. 400 nm that corresponds to excitation into upper-lying excited singlet states.[47] Unlike the case in fluid solution, the solid-state spectrum shows notable absorption at longer wavelength (Figure S0). This latter feature is rather indistinct and lacks an obvious maximum while the absorption onset is at around 625 nm. Excitation spectra recorded for the crystals are better defined and indicate the presence of two absorbing species (Figure 7). One such species retains the spectral features normally associated with BODIPY-based chromophores,[1-4] with a maximum at 524 nm and a vibronic progression at higher energies. This transition corresponds to the dominant band seen in the absorption spectrum. The second species shows a split excitation spectrum (Figure 7) consistent with excitonic interactions between adjacent dipyrrin units.[48] In this latter case, the two maxima appear at *ca*. 555 and *ca*. 490 nm, corresponding to a crude estimate for the splitting energy of ca. 1,390 cm^{-1}. The lower-energy transition is more favoured but the underlying absorption bands are relatively broad.

Both absorbing species identified for crystalline **2** are emissive in the solid state (Figure 7). The species subject to excitonic coupling can be selectively excited at wavelengths around 560 nm. The resultant emission has a maximum at 635 nm and a fluorescence lifetime of 4.4 ± 0.3 ns. This fluorescence is clearly associated with the lower-energy transition noted for the aggregated species. In contrast, excitation into the second species at 500 nm gives strong emission centred at *ca*. 550 nm, together with weaker fluorescence from the aggregate. The dominant emitting species has a fluorescence lifetime of 1.00 ± 0.05 ns and is attributed to a monomeric chromophore in the bulk crystal. The amount of longer-lived component observed following excitation at 525 nm is around 25% and is considered far too high to accurately reflect the relative absorption (or excitation) profiles (Figure 7b). This would suggest that electronic energy transfer occurs from the discrete chromophore to the aggregate within the crystal, for which the excitation spectrum provides strong support. The total fluorescence quantum yield measured following excitation of the crystal at 525 nm is *ca*. 0.09, as measured with an integrating sphere.

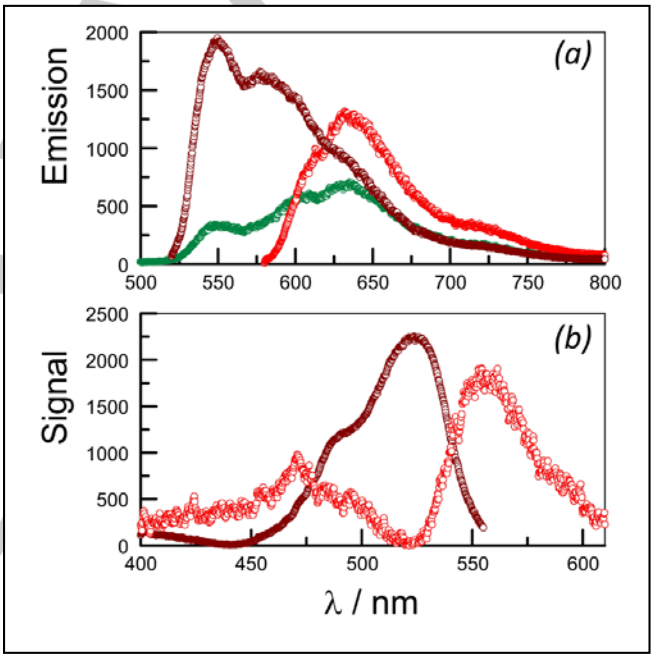

Figure 7. (a) Examples of fluorescence spectra recorded for single crystals of **2** with excitation at 500 (brown circles), 480 (green circles), and 560 nm (red circles), (b) Examples of excitation spectra recorded for **2** with emission detection at 580 (brown circles) and 680 nm (red circles).

The overall situation for solid-state emission from **2** is illustrated pictorially by way of Scheme 2. Here, it is assumed that the crystal comprises ordered columns of arranged molecules of **2** separated by less ordered domains. The aligned columns are able to facilitate electronic energy migration between adjacent chromophores. In this way, the exciton can sample many different chromophores before undergoing deactivation. Excitons arriving at an interfacial zone, where aggregation could be favoured by the amorphous state, will be trapped by the emissive dimer. There is good spectral overlap to drive this exciton trapping process.

This provides an easy route for enhanced emission from the dimer, which need be present only at low concentration.

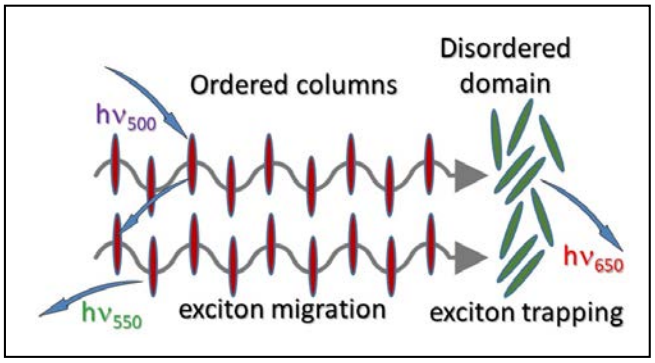

Scheme 2. Pictorial representation of the putative exciton migration and trapping proposed for crystalline **2.** According to our model, photons are absorbed by chromophores arranged in columns within the bulk crystal. The columns favour fast exciton migration along the columns with occasional passage to an adjacent column. It is further proposed that the crystalline regions are in contact with more disordered domains that allow aggregation (or dimerization) to occur. There is a strong driving force for electronic energy transfer from the crystalline phase to the more amorphous phase, with subsequent fluorescence from the aggregate. A similar situation holds for **3** and for the two bichromophores.

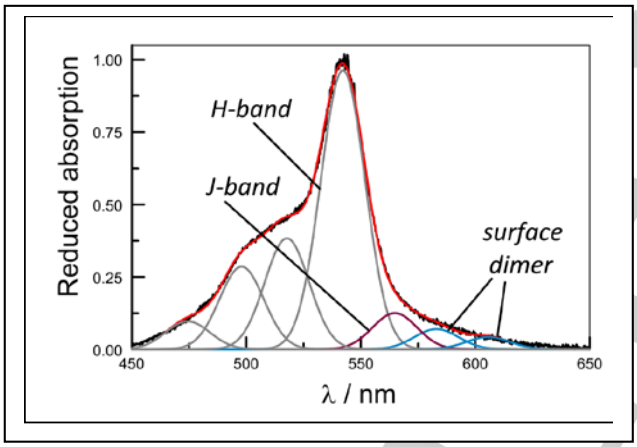

Figure 8. Absorption (black curve) and simulated absorption (red curve) spectra for crystalline **BC2**. The individual components associated with the Gaussian line-shape deconstruction are shown below the spectra. The grey and plum curves, respectively, are assigned to the H- and J-bands. The residual absorption at long wavelength (blue curves) is attributed to aggregated states residing at an interface or in a somewhat amorphous phase.

The absorption spectrum recorded for a single crystal of **BC2** shows a maximum at 545 nm but with quite pronounced absorption at longer wavelengths (Figure 8). Excitation to higher-lying singlet states is seen at around 390 nm.[47] The absorption profile in the 450-460 nm window can be analysed in terms of Gaussian components with the aid of the crystallographic data (Figure 8). Thus, the pair of chromophores identified as the main species in the crystal lattice approximate to Kasha's model[41] for parallel transition dipole moments. This arrangement would give rise to a strong H-band in the absorption spectrum. However, the slight offset between the dipole vectors allows absorption to the corresponding J-band. Our analysis of the absorption spectrum places the origin of the H-band at 18,445 cm^{-1} and that of the J-band at 17,705 cm^{-1}. The excitonic splitting, therefore, is 740 cm^{-1}. The ratio of oscillator strengths (N) is *ca*. 13 in favour of the H-band, which can be compared with the value (N = 10) calculated[49] using the X-ray structural data. The absorption spectrum also indicates weak transitions centred at 606 and 583 nm which are most likely due to aggregated species associated with molecules residing in a somewhat amorphous domain (Figure 8).

Two overlapping fluorescence profiles can be resolved for single crystals of **BC2** (Figure 9). Thus, excitation at 580 nm gives rise to a sharp fluorescence spectrum having a well-defined maximum at 610 nm. This emission is most likely associated with the aggregated species assigned to an interfacial domain and has a fluorescence lifetime of 5.7 ± 0.2 ns. In contrast, excitation at wavelengths around 510 nm gives an emission spectrum exhibiting maxima at 563 and 605 nm. The latter band is the same as that found following excitation at 580 nm, while the component with a maximum at 563 nm has a fluorescence lifetime of 0.85 ± 0.05 ns. Excitation spectra recorded for fluorescence from the shorter-lived species correspond to the chromophore absorbing primarily at 545 nm (Figure S0). However, excitation spectra recorded for emission from the aggregated species are fully consistent with a combination of direct excitation into the aggregate and electronic energy transfer from the bulk chromophore (Figure S0).

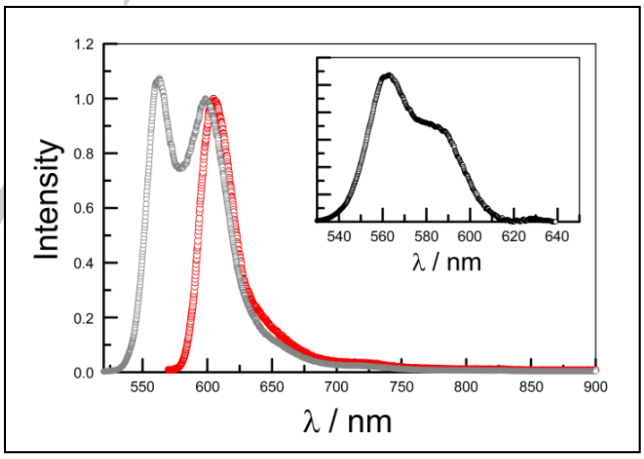

Figure 9. Fluorescence spectra recorded for single crystals of **BC2** following excitation at 580 nm (red circles) and 510 nm (Grey circles). The insert shows the fluorescence profile for the J-species as determined by iterative reconstruction of the two spectra.

It is apparent that fluorescence from the crystal is subject to very small Stokes shifts.[50] This seems reasonable on the grounds that there are no possible solvent effects and the crystal lattice will prevent any geometrical changes accompanying relaxation of the excited state. The H-species does not emit but (presumably) undergoes fast internal conversion to populate the corresponding J-species. The latter emits but, because of the

decreased oscillator strength relative to the conventional BODIPY core, possesses a lower k_{RAD}. Direct excitation into the H-band, where the interface-facilitated aggregate appears not to absorb, leads to fluorescence from the aggregate. This situation requires electronic energy transfer from the bulk material to molecules within the interfacial domain.[51] There is good spectral overlap between emission from the J-species and absorption by the aggregate (Figure S0), which should help promote dipole-dipole electronic energy transfer. Likewise, the small Stokes shift should facilitate fast Coulombic-type exciton migration between pairs of **BC2** chromophores occupying columns within the bulk crystal (see Supporting Information).

For **2**, the transition dipole moment[52] has a value of 2.8 D while the electronic coupling matrix element, which includes the orientation factor, for dipole-dipole interactions within the crystal, as calculated by the Kuhn extended dipole approach,[40] is 40 cm^{-1}. The spectral overlap integral for bulk **2** is only 0.0005 cm, despite the small Stokes shift imposed by the lattice. These terms, which refer exclusively to Coulombic interactions, allow estimation of the rate constant for electronic energy transfer between adjacent **2** molecules along a column as being 7 x 10^{11} s^{-1} (see Supporting Information). Of course, energy transfer along the chain will resemble a random walk[45] with occasional passage to other chains. None-the-less, it is clear that the exciton could sample many hundreds of different molecules within its lifetime of 1 ns. This easy diffusion along the chain will be interrupted by exciton trapping by the aggregate. The same calculation made for **BC2** indicates a rate constant for energy transfer between adjacent pairs of ca. 2 x 10^{11} s^{-1}.

Conclusions

Quantitative fluorescence measurements with single crystals formed from organic fluorophores are both demanding and rewarding. The design criteria for engineering strongly emissive crystals are not yet understood or even properly defined. Progress is being made, however, and certain observations point the way forward.[13] For example, it is shown here that the crystal lattice curtails radiationless decay promoted *via* rotational processes and thereby enhances the likelihood for radiative decay of the excited state. Bulky substituents can help minimize π,π interactions by imposing isolation of the chromophores and by causing slight offset of the columns. Fluorophores within the lattice assemble into unpredictable ensembles that can introduce new electronic structures, such as the pairs of chromophores found here with **BC2**. A real advantage offered by photonic crystals is the capability for exciton migration over hundreds of individual units assembled to form a stack. Obtaining the same capability by way of covalent connections is essentially impossible[53] and this simple realization makes the crystals important candidates for use as artificial light-harvesting arrays.

Photonic crystals[51] obtained from BODIPY-based substances appear to form an amorphous domain, or deposit, as an interface with the ordered crystalline columns. These relatively disordered regions offer the possibility to assemble different types of intermolecular species with closer interactions than found in the ordered columns. Indeed, molecules in the interfacial domain can fom dimers, or higher aggregates, that absorb and emit at relatively long wavelength. This, in turn, provides the driving force to trap excitons migrating along the columns, with the latter acting as photon antennae. Our studies indicate that the aggregates can possess quite long-lived excited states and are therefore possible candidates as energy donors for opto-electronic devices. Constructing such systems represents the next phase of this project.

A separate point to emerge from this investigation concerns the apparent inhibition of the barrier crossing observed for **2** on moving to the bichromophore. This situation is highly unexpected and, as far as we can see, unprecedented. Overall, it appears that the potential energy surface for the excited state of the bichromophore is less porous than that of the corresponding mono-chromophore. This could be a consequence of electronic interactions or steric crowding but our results do not allow discrimination between these effects. It is, however, an important observation that merits further investigation.

Experimental Section

Synthesis of 2 and BC2: PhLi (0.6 mL of a 1.8 M solution in di-*n*-butyl ether, 1.08 mmol) was added using a syringe under a nitrogen atmosphere to a 25 mL round-bottom Schlenk flask containing a solution of 8-chlorophenyl-BODIPY (50 mg, 0.121 mmol) dissolved in dry toluene (1.5 mL). After 15 min, TLC analysis (petroleum ether/CH_2Cl_2, 70:30) revealed completion of the reaction. Then, the dark-red coloured reaction mixture was diluted with CH_2Cl_2 (50 mL) and washed with brine (3 x 100 mL). The combined organic layers were dried over Na_2SO_4 and concentrated *in vacuo*. The residue was purified by column chromatography (SiO_2, petroleum ether/CH_2Cl_2, 70:30) to afford **2** as an orange solid (13 mg, 20%). ^{1}H NMR (300 MHz, $CDCl_3$) δ ppm: 7.50 (d, *J* = 8.5 Hz, 2H), 7.42-7.38 (m, 4H), 7.32 (d, *J* = 8.5 Hz, 2H), 7.28-7.16 (m, 6H), 2.24 (q, *J* = 7.6 Hz, 4H), 1.78 (s, 6H), 1.36 (s, 6H), 0.92 (t, *J* = 7.4 Hz, 6H). ^{13}C NMR ($CDCl_3$, 100 MHz) δ ppm: 153.3, 139.0, 135.5, 135.0, 134.5, 133.8, 133.0, 130.6, 130.4, 129.0, 127.1, 125.5, 17.3, 14.7, 14.5, 12.2. A second dark-red coloured compound was obtained in this reaction as the major product **BC2** (32 mg, 50%). ^{1}H NMR (300 MHz, $CDCl_3$) δ ppm: 7.46 (d, *J* = 8.5 Hz, 4H), 7.26 (d, *J* = 8.3 Hz, 4), 7.22-7.16 (m, 20H), 2.22 (q, *J* = 7.6 Hz, 4H), 1.76 (s, 6H), 1.46-1.36 (m, 8H), 1.32 (s, 6H), 1.13 (s, 6H), 0.91 (t, *J* = 7.6 Hz, 6H). 0.61 (t, *J* = 7.5 Hz, 6H). ^{13}C NMR ($CDCl_3$, 100 MHz) δ ppm: 156.9, 153.0, 138.9, 135.6, 135.0, 134.9, 134.7, 134.4, 133.6, 133.0, 130.9, 130.4, 130.3, 129.0, 127.2, 125.4, 25.5, 17.3, 16.0, 14.9, 14.8, 14.6, 12.2, 12.1.

Synthesis of 3 and BC3: A solution of 1.05 equivalent of *n*-BuLi (2.5 M in hexane, 3.2 mL) was added dropwise to a solution of 1,4-dibromobenzene (1.89 g, in dry toluene, 4.3 mL) in a 25 mL round-bottom Schlenk flask under a nitrogen atmosphere and the resulting mixture was stirred at 50 °C for 2 h. Then 0.5 mL of this stock solution was transferred using a syringe to a 25 mL round-bottomed Schlenk flask containing 8-chlorophenyl-BODIPY (**1**) (50 mg, 0.121 mmol) dissolved in dry toluene (1.5 mL) under a nitrogen atmosphere. After 15 min, TLC analysis (petroleum ether/CH_2Cl_2, 70:30) revealed completion of the reaction. The dark-red reaction mixture was diluted with CH_2Cl_2 (50 mL) and washed with brine (3 x 100 mL). The combined organic layers were dried over Na_2SO_4 and concentrated *in vacuo*. The residue was purified by column chromatography (SiO_2, petroleum ether/CH_2Cl_2, 70:30) to afford **3** as an orange solid (20 mg, 25%). ^{1}H NMR (300 MHz, $CDCl_3$) δ ppm: 7.41 (d, *J* = 8.5 Hz, 2H), 7.28 (d, *J* = 8.3 Hz, 4H), 7.20 (d, *J* = 8.4 Hz, 2H), 7.11 (d, *J* =

8.3 Hz, 4H), 2.17 (q, *J* = 7.6 Hz, 4H), 1.66 (s, 6H), 1.26 (s, 6H), 0.82 (t, *J* = 7.5 Hz, 6H). A second dark-red coloured compound was obtained in this reaction as the major product **BC3** (46 mg, 55%). ^{1}H NMR (300 MHz, $CDCl_3$) δ ppm: 7.39 (d, *J* = 8.3 Hz, 4H), 7.24 (d, *J* = 8.2 Hz, 8), 7.15 (d, *J* = 8.3 Hz, 4H), 6.91 (d, *J* = 7.8 Hz, 8H), 2.14 (q, *J* = 7.5 Hz, 4H), 1.65 (s, 6H), 1.40-1.30 (m, 8H), 1.24 (s, 6H), 1.13 (s, 6H), 0.81 (t, *J* = 7.5 Hz, 6H). 0.53 (t, *J* = 7.3 Hz, 6H).

Spectroscopic studies: Spectroscopic-grade solvents were purchased from commercial sources and used as received after ensuring the absence of fluorescent impurities. Absorption spectra were recorded with a Hitachi U-3310 spectrophotometer while steady-state fluorescence studies were made with an Yvon-Jobin Fluorolog tau-4 spectrometer. Fluorescence quantum yields were determined by reference to known standards used at optically dilute concentrations. The main fluorescence standard was Fluorescein in 0.1M NaOH solution (Φ_F = 0.91 ± 0.05), with excitation at 500-510 nm.[54] Ancillary reference systems included Rhodamine 6G in ethanol (Φ_F = 0.94 ± 0.03).[55] Corrections were made for changes in refractive index.[56] Fluorescence lifetimes were recorded by time-correlated, single photon counting methods with high intensity, short duration laser diodes as excitation source. These diodes provided discrete excitation wavelengths of 510 nm (FWHM = 130 ps), 560 nm (FWHM = 100 ps) and 635 nm (FWHM = 130 ps). Fluorescence was isolated from scattered excitation light using a high-radiance monochromator and detection was made with a micro-channel plate PMT operated at -20 ^{0}C. Data analysis was made by standard statistical methods. Temperature dependence studies were made with an Oxford Instruments Optistat DN using dilute solutions of the fluorophore in fresh MTHF solution. Higher temperature studies were made with a Harricks' demountable liquid cell and temperature controller.

Structural studies: ^{1}H and 13C NMR spectra were recorded in fully deuterated solvents at 298K on a Bruker Avance III HD 500 MHz spectrometer. Alternatively, spectra were recorded with a Bruker 700 Avance III HD NMR spectrometer operating at 700.13 MHz. This spectrometer is equipped with a triple-resonance nitrogen cooled cryoprobe prodigyTM for temperature-dependence studies. The same instrument was used to record COSY, NOESY, ROESY, HSQC and HMBC spectra. All crystal structural data were collected using copper radiation (λCuKα = 1.54184 Å) on an Xcalibur, Atlas, Gemini Ultra diffractometer equipped with an Oxford Cryosystems CryostreamPlus open-flow N_2 cooling device. For **BC2** and **3**, the intensities were corrected for absorption using a multifaceted crystal model created by indexing the faces of the crystal for which data were collected.[57] For **2** and **BC3**, the intensities were corrected for absorption empirically using spherical harmonics. Data were collected at 150K except in the case of **BC3** for which data were collected at 240K as crystals of this compound underwent a phase transition at lower temperatures. Cell refinement, data collection and data reduction were undertaken via the software CrysAlisPro.[58] Structures were solved using XT[59] and refined by XL[60] using the Olex2 interface.[61] All non-hydrogen atoms were refined anisotropically and hydrogen atoms were positioned with idealized geometry. The displacement parameters of the hydrogen atoms were constrained using a riding model with $U_{(H)}$ set to be an appropriate multiple of the U_{eq} value of the parent atom.

For the optical studies, crystals were suspended on a rotatable stage and carefully positioned in the excitation beam. Once aligned, the stage was isolated from stray light and maintained at 20 ^{0}C. A notch filter was used to exclude excitation light and emission was directed to the spectrophotometer via optical fibres. For absorption spectra, a few crystals were deposited onto a clean quartz plate and spectra recorded using optical fibres to connect with the instrument. Fluorescence quantum yields were measured using an integrating sphere (StellaNet) and the procedure recommended by Beeby *et al*.[62]

Computational studies: Spectral deconstruction of reduced absorption or fluorescence spectra was made with PEAKFIT. The minimum number of Gaussian profiles needed to accurately reproduce the entire spectral envelop was used for the analysis. Quantum chemical calculations were made with TURBOMOLE. Structural studies were made at the DFT level using the B3LYP functional and with the PBE0 basis set. Solvent effects were modelled using the PCM approach with PCM($CHCl_3$) with the Mennucci-Tomasi correction. Rotational studies were made by semi-empirical methods using AMPAC-10 and the COSMO model for solvent effects. These calculations used the non-rigid chain method with the DFT optimized initial and final geometries.

Acknowledgements

We thank Newcastle University for financial support and TUBITAK-BIDEB (2219-1059B191701080) for the award of a Research Scholarship to OAB. HHTA-S gratefully acknowledges the award of a postgraduate scholarship from The Umm Al-Qura University (Saudi Arabia).

Keywords: BODIPY dyes • photophysics • fluorescence • solid state • aggregation

[1] a) G. Ulrich, R. Ziessel, A. Harriman, *Angew. Chem., Int. Ed*. **2008**, *47*, 1184-1201. b) R. Ziessel, G. Ulrich, A. Harriman, *New J. Chem*. **2007**, *31*, 496-501.

[2] a) A. Loudet, K. Burgess, *Chem. Rev*. **2007**, *107*, 4891-4932. b) N. Boens, V. Leen, W. Dehaen, *Chem. Soc. Rev*. **2012**, *41*, 1130-1172.

[3] a) H. Lu, J. Mack, Y. C. Yang, Z. Shen, *Chem. Soc. Rev*. **2014**, *43*, 4778-4823. b) A. C. Benniston, G. Copley, *Phys. Chem. Chem. Phys*. **2009**, *11*, 4124-4131.

[4] a) O. A. Bozdemir, S. Erbas-Cakmak, O. O. Ekiz, A. Dana, E. U. Akkaya, *Angew. Chem., Int. Ed*. **2011**, *50*, 10907-10912. b) A. B. Nepomnyashchill, A. J. Bard, *Acc. Chem. Res*. **2012**, *45*, 1844-1853.

[5] a) F. Würthner, T. E. Kaiser, C. R. Saha-Moeller, *Angew. Chem., Int. Ed*. **2011**, *50*, 3376-3410. b) B. Le Guennic, D. Jacquemin, *Acc. Chem. Res*. **2015**, *48*, 530-537.

[6] a) Y. Ni, J. Wu, *Org. Biomol. Chem*. **2014**, *12*, 3774-3791. b) J. N. Bai, R. E. Pagano, *Biochem*. **1997**, *36*, 8840-8848. c) S. L. Niu, G. Ulrich, R. Ziessel, A. Kiss, P. Y. Renard, A. Romieu, *Org. Lett*. **2009**, *11*, 2049-2052. d) X. F. Zhang, Y. Xiao, J. Qi, J. L. Qu, B. Kim, X. L. Yue, K. D. Belfield, *J. Org. Chem*. **2013**, *78*, 9153-9160.

[7] a) N. N. Kim, W. X. Ren, J. S. Kim, J. Yoon, *Chem. Soc. Rev*. **2012**, *41*, 3210-3244. b) H. Sunahara, Y. Urano, H. Kojima, T. Nagano, *J. Am. Chem. Soc*. **2007**, *129*, 5597-5604. c) J. Y. Shao, H. Y. Sun, H. M. Guo, S. M. Ji, J. Z. Zhao, W. Y. Wu, X. L. Yuan, C. L. Zhang, T. D. James, *Chem. Sci*. **2012**, *3*, 1049-1061. d) R. Ziessel, G. Ulrich, A. Harriman, M. A. H. Alamiry, B. Stewart, P. Retailleau, *Chem. Eur. J*. **2009**, *15*, 1359-1369.

[8] a) Y. Ge, D. F. O'Shea, *Chem. Soc. Rev*. **2016**, *45*, 3846-3864. b) E. A. Leushina, I. A. Usol'tsev, S. I. Bezzubov, A. A. Moiseeva, M. V. Terenina, A. V. Anisimov, I. V. Taydakov, A. V. Khoroshutin, *Dalton Trans*. **2017**, *46*, 17093–17100. c) N. Wang, Y. Wang, J. Gao, X. Ji, J. He, J. Zhang, W. Zhao, *Analyst*, **2018**, *143*, 5728–5735.

[9] a) R. Misra, B. Dhokale, T. Jadhav, S. M. Mobin, *New J. Chem*. **2014**, *38*, 3579-3585. b) I. Esnal, I. Valois-Escamilla, C. F. A. Gomez-Duran, A. Urias-Benavides, M. L. Betancourt-Mendiola, I. Lopez-Arbeloa, J. Banuelos, I. Garcia-Moreno, A. Costela, E. Pena-Cabrera,

ChemPhysChem **2013**, *14*, 4134-4142. c) K. Kim, C. Jo, S. Easwaramoorthi, J. Sung, D. H. Kim, D. G. Churchill, *Inorg. Chem*. **2010**, *49*, 4881-4894.

[10] a) R. Ziessel, C. Goze, G. Ulrich, *Synthesis – Stuttgart* **2007**, 936-949. b) S. Goeb, R. Ziessel, *Org. Lett*. **2007**, *9*, 737-740. c) C. Goze, G. Ulrich, R. Ziessel, *J. Org. Chem*. **2007**, *72*, 313-322. d) A. Harriman, G. Izzet, R. Ziessel, *J. Am. Chem. Soc*. **2006**, *128*, 10868-10875.

[11] a) R. Clarke, K. L. Ho, A. A. Alsimaree, O. J. Woodford, P. G. Waddell, J. Bogaerts, W. Herrebout, J. G. Knight, R. Pal, T. J. Penfold, M. J. Hall, *ChemPhotoChem* **2017**, *1*, 513-517. b) R. B. Alnoman, S. Rihn, D. C. O'Connor, F. A. Black, B. Costelo, P. G. Waddell, W. Clegg, R. D. Peacock, W. Herrebout, J. G. Knight, M. J. Hall, *Chem. Eur. J.* **2016**, *22*, 96-96.

[12] a) Y. J. Cui, J. Zhang, H. J. He, G. D. Qian, *Chem. Soc. Rev*. **2018**, *47*, 5740-5785. b) S. Furumi, *Polym. J*. **2013**, *45*, 579-593. c) R. Cheriya, K. Nagarajan, M. Hariharan, *J. Phys. Chem. C* **2013**, *117*, 3240-3248. d) U. Venkataramudu, M. Annadhasan, H. Maddali, R. Chanrasekar, *J. Mater. Chem*. **2017**, *5*, 7262-7269.

[13] a) L. Jiang, H. Gao, L. Z. Gai, Z. Shen, *New J. Chem*. **2018**, *42*, 8271-8275. b) R. P. Paitandi, R. S. Singh, B. K. Dwivedi, V. D. Singh, D. S. Pandey, *Dalton Trans*. **2018**, *47*, 3785-3795. c) D. Sirbu, A. C. Benniston, A. Harriman, *Org. Lett*. **2017**, *19*, 1626-1629. d) H. A. A. El-Ali, J. Jing, X. L. Zhanh, *RSC Adv*. **2019**, *9*, 16246-16251. e) C. Duan, Y. B. Zhou, G. G. Shan, Y. C. Chen, W. J. Zhao, D. D. Yuan, L. T. Zeng, X. B. Huang, G. L. Niu, *J. Mater. Chem*. **2019**, *7*, 3471-3478. f) Y. Liu, L. Y. Niu, X. L. Liu, P. Z. Chen, Y. S. Yao, Y. Z. Chen, Q. Z. Yang, *Chem. Eur. J*. **2018**, *24*, 13549-13555. g) D. Tian, F. Qi, H. L. Ma, X. Q. Wang, Y. Pan, R. F. Chen, Z. Shen, Z. P. Liu, L. Huang, W. Huang, *Nature Commun*. **2018**, *9*, 2688. h) Y. Y. Liao, S. T. A. G. Melissen, J. F. Audibert, T. T. Vu, G. Clavier, R. Meallet-Renault, P. Retailleau, J. P. Lemaistre, V. Genot, R. Pansu, *ChemPhotoChem* **2018**, *2*, 72-80. i) C. Maeda, T. Todaka, T. Ueda, T. Ema, *Org. Biomol. Chem*. **2017**, *15*, 9283-9287.

[14] a) N. Aratani, D. Kim, A. Osuka, *Acc. Chem. Res*. **2009**, *42*, 1922-1934. b) R. Ziessel, G. Ulrich, A. Haefele, A. Harriman, *J. Am. Chem. Soc*. **2013**, *135*, 11330-11344. c) J. S. Hsiao, B. F. Krueger, R. W. Wagner, T. E. Johnson, J. K. Delaney, D. C. Mauzerall, G. R. Fleming, J. S. Lindsey, D. F. Bocian, R. J. Donohoe, *J. Am. Chem. Soc*. **1996**, *118*, 11181-11893. d) D. Gust, T. A. Moore, A. L. Moore, *Acc. Chem. Res*. **2001**, *34*, 40-48.

[15] G. McDermott, S. M. Prince, A. A. Freer, A. M. Hawthornthwaite-Lawless, M. Z. Papiz, R. J. Cogdell, N. W. Issacs, *Nature* **1995**, *374*, 517-521.

[16] a) W. X. Zhang, W. L. Sheng, C. J. Yu, Y. Wei, H. Wang, E. H. Hao, L. J. Jiao, *Chem. Commun*. **2017**, *53*, 5318-5321. b) T. T. Li, W. Gu, C. J. Yu, X. K. Lv, H. Wang, E. H. Hao, L. J. Jiao, *Chin. J. Chem*. **2016**, *34*, 989-996. c) R. Sharma, H. B. Gobeze, F. D'Souza, M. Ravikanth, *ChemPhysChem* **2016**, *17*, 2516-2524. d) J. Ahrens, A. Scheja, R. Wicht, M. Bröring, *Eur. J. Org. Chem*. **2016**, 2864-2870. e) J. Ahrens, B. Böker, K. Brandhorst, M. Funk, M. Bröring, *Chem. Eur. J*. **2013**, *19*, 11382-11395.

[17] a) J. Z. Zhao, K. P. Chen, Y. Q. Hou, Y. Y. Che, L. Liu, D. Z. Jia, *Org. Biomol. Chem*. **2018**, *16*, 3692-3701. b) X.-F. Zhang, *J. Photochem. Photobiol. A Chem*. **2018**, *355*, 431-443. c) Y. Liu, J. Z. Zhao, A. Iagatti, L. Bussotti, P. Foggi, E. Castellucci, M. Di Donato, K. L. Han, *J. Phys. Chem. C* **2018**, *122*, 2502-2511. d) R. Montero, V. Martinez-Martinez, A. Longarte, N. Epelde-Elezcano, E. Palao, I. Lamas, H. Manzano, A. R. Agarrabestia, K. Arbeloa, M. J. Ortiz, *J. Phys. Chem. Lett*. **2018**, *9*, 641-646.

[18] a) Y. Hayashi, S. Yamaguchi, W. Y. Cha, D. Kim, H. Shinokubo, *Org. Lett.* **2011**, *13*, 2992-2995. b) Y. Cakmak, E. U. Akkaya, *Org. Lett*. **2009**, *11*, 85-88. c) M. Zhu, L. Jiang, M. Yuan, X. Liu, C. Ouyang, H. Zheng, X. Yin, Z. Zuo, H. Liu, Y. Li, *J. Polym. Sci., Part A: Polym. Chem*. **2008**, *46*, 7401-7410. d) S. Rihn, M. Erdem, A. De Nicola, P. Retailleau, R. Ziessel, *Org. Lett*. **2011**, *13*, 1916-1919.

[19] a) T. Rohand, M. Baruah, W. Qin, N. Boens, W. Dehaen, *Chem. Commun*. **2006**, 266-268. b) T. Rohand, W. Qin, N. Boens, W. Dehaen, *Eur. J. Org. Chem*. **2006**, 4658-4663. c) M. Baruah, W. Qin, N. Basaric, W. M. De Borggraeve, N. Boens, *J. Org. Chem*. **2005**, *70*, 4152-4157. d) M. Shah, K. Thangaraj, M. L. Soong, L. T. Wolford, J. H. Boyer, I. R. Politzer, T. G. Pavlopoulos, *Heteroatom Chem*. **1990**, *1*, 389-399. e) V. Leen, E. Braeken, K. Luckermans, C. Jackers, M. Van der Auweraer, N. Boens, W. Dehaen, *Chem. Commun*. **2009**, 4515-4517.

[20] a) V. Leen, V. Zaragozı´Gonzalvo, W. M. De Borggraeve, N. Boens, W. Dehaen, *Chem. Commun*. **2010**, *46*, 4908–4910. b) M. Makosza, K. Wojciechowski, *Chem. Rev*. **2004**,*104*, 2631–2666. c) V. Leen, M. Van der Auweraer, N. Boens, W. Dehaen, *Org. Lett*. **2011**, *13*, 1470-1473.

[21] a) T. Dohi, M. Ito, N. Yamaoka, K. Morimoto, H. Fujioka, Y. Kita, *Tetrahedron* **2009**, *65*, 10797-10815. b) H. Yamane, S. Ito, K. Tanaka, Y. Chujo, *Polym. Chem*. **2016**, *7*, 2799-2807.

[22] E. Bodio, C. Goze, *Dyes Pigm*. **2019**, *160*, 700-710.

[23] a) A. Haefele, G. Ulrich, P. Retailleau, R. Ziessel, *Tetrahedron Lett*. **2008**, *49*, 3716-3721. b) A. Harriman, L. J. Mallon, K. J. Elliot, A. Haefele, R. Ziessel, *J. Am. Chem. Soc*. **2009**, *131*, 13375-13386.

[24] a) M. L. Lepage, A. Mirloup, M. Ripoll, F. Stauffert, A. Dodlenner, R. Ziessel, P. Compain, *Beilstein, J. Org. Chem*. **2015**, *11*, 659-667. b) S. Niu, G. Ulrich, P. Retailleau, R. Ziessel, *Org. Lett*. **2011**, *13*, 4996-4999.

[25] C. Goze, G. Ulrich, L. J. Mallon, B. D. Allen, A. Harriman, R. Ziessel, J. Am. Chem. Soc. 2006, 128, 10231-10239.

[26] a) K. Huang, A. Rhys, *Proc. Roy. Soc. London Ser. A* **1950**, *204*, 406-423. b) A. Felouat, A. D'Aleo, F. Fages, *J. Org. Chem*. **2013**, *78*, 4446-4455. c) F. A. C. Oliveira, L. A. Curry, A. Righi, R. L. Moreira, P. S. S. Guimaraes, F. M. Matinaga, M. A. Pimenta, R. A. Nogueira, *J. Chem. Phys*. **2003**, *119*, 9777-9782.

[27] H. Mustroph, A. Towns, *ChemPhysChem* **2018**, *19*, 1016-1023.

[28] M. A. H. Alamiry, E. Baidarah, A. Harriman, J. H. Olivier, R. Ziessel, *Pure Appl. Chem.* **2013**, *85*, 1349-1365.

[29] S. J. Strickler, R. A. Berg, *J. Chem. Phys*. **1962**, *37*, 814-83-22.

[30] G. Ulrich, C. Goze, S. Goeb, P. Retailleau, R. Ziessel, *New J. Chem*. **2006**, *30*, 982-986.

[31] H. Gao, Y. Gao, C. Wang, D. Hu, Z. Xie, L. Liu, B. Yang, Y. Ma, *ACS Appl. Mater. Interfaces* **2018**, 000.

[32] J. W. Verhoeven, Sigma-coupled Charge-Transfer Probes of the Fluoroprobe and Fluorotype Type. In Topics of Fluorescence Spectroscopy (G. D. Geddes and J. R. Lakowirz, Eds.) Springer, Boston, 2005, Vol. 9.

[33] R. Al-Aqar, A. C. Benniston, A. Harriman, T. Perks, *ChemPhotoChem* **2017**, *1*, 198-205.

[34] A. Messaadi, N. Dhouibi, H. Hamda, F. B. M. Belgacem, Y. H. Adbelkader, N. Ouerfelli, A. H. Hamzaoui, *J. Chem*. **2015**, 163262.

[35] P. D. Zoon, A. M. Brouwer, *Photochem. Photobiol. Sci*. **2009**, *8*, 345-353.

[36] E. Görlach, H. Gygax, P. Lubini, U. Wild, *Chem. Phys*. **1995**, *194*, 185-193.

[37] P. Stachelek, A. Harriman, *J. Phys. Chem. A* **2016**, *120*, 8104-8113.

[38] a) J. E. I. Korppi-Tommola, A. Hakkarainen, T. Hukka, J. Subbi, *J. Phys. Chem.* **1991**, *95*, 8482-8491. b) V. Sundstrom, T. Gillbro, *J. Phys. Chem*. **1982**, *86*, 1788-1794.

[39] a) N. Saki, T. Dinc, E. U. Akkaya, *Tetrahedron* **2006**, *62*, 2721-2725. b) F. Bergstrom, I. Mikhalyov, P. Hagglof, *J. Am. Chem. Soc*. **2002**, *124*, 196-204. c) A. C. Benniston, G. Copley, A. Harriman, D. Howgego, R. W. Harrington, W. Clegg, *J. Org. Chem*. **2010**, *75*, 2018-2027. d) M. Bröring, R. Krueger, S. Link, C. Kleeberg, S. Khoehler, X. Xie, B. Ventura, L. Flamigni, *Eur. J. Chem*. **2008**, *14*, 2976-2983.

[40] V. Czikkely, H. D. Forsterling, H. Kuhn, *Chem. Phys. Lett*. **1970**, *6*, 207-210.

[41] M. Kasha, H. R. Rawls, M. Ashraf El-Bayoumi, *Pure Appl. Chem*. **1965**, *11*, 371-392.

[42] D. Sirbu, J. K. G. Karlsson, A. Harriman, *J. Phys. Chem. A* **2018**, *122*, 9160-9170.

[43] a) A. Prly, L. Vannay, C. Corminboeuf, *Helv. Chim. Acta* **2017**, *100*, e1700093. b) A. Prly, L. Vannay, C. Corminboeuf, *Phys. Chem. Chem. Phys*. **2016**, *18*, 32668-32672.

[44] F. Bergstrom, I. Mikhalyov, P. Hagglof, R. Wortmann, T. Ny, L. B. A. Johansson, *J. Am. Chem. Soc*. **2002**, *124*, 196-204.

[45] a) D. L. Andrews, *J. Nanophotonics* **2008**, *2*, 022502. b) D. L. Andrews, G. D. Scholes, C. Curutchet, *Laser Photonics Rev*. **2011**, *5*, 114-123. c) H. Sigal, D. Markovitsi, L. K. Gallos, P. Argyrakis, *J. Phys. Chem*. **1996**, *100*, 10999-11004.

[46] D. Hablot, R. Ziessel, M. A. H. Alamiry, E. Bahraidah, A. Harriman, *Chem. Sci*. **2013**, *4*, 444-453.

[47] G. J. Hedley, A. Ruseckas, A. Harriman, I. D. W. Samuel, *Angew. Chem., Int. Ed.* **2011**, *50*, 663.4-6637.

[48] F. Würthner, C. R. Saha-Moller, B. Fimmel, S. Ogi, P. Leowanawat, D. Schmidt, *Chem. Rev*. **2016**, *116*, 962-1052.

[49] a) K. J. Thorley, F. Würthner, *Org. Lett*. **2012**, *14*, 6190-6193. b) M. Son, K. H. Park, C. Shao, F. Würthner, D. Kim, *J. Phys. Chem. Lett*. **2014**, *5*, 3601-3607.

[50] H. Langhals, O. Krotz, K. Polborn, P. Mayer, *Angew. Chem., Int. Ed*. **2005**, *44*, 2427-2428.

[51] R. Al-Aqar, A. Atahan, A. C. Benniston, T. Perks, P. G. Waddell, A. Harriman, *Chem. Eur. J*. **2016**, *22*, 15420-15429.

[52] I. Renge, *J. Phys. Chem*. **1993**, *97*, 6582-6589.

[53] a) J. Seth, V. Palaniappan, T. E. Johnson, S. Prathapan, J. S. Londsey, D. F. Bocian, *J. Am. Chem. Soc*. **1994**, *116*, 10578-10592. b) A. Harriman, R. Ziessel, *Chem. Commun*. **1996**, 1707-1716. c) A. Harriman, R. Ziessel, *Chem. Commun*. **2011**, *47*, 611-631.

[54] D. F. Eaton, *Pure Appl. Chem*. **1988**, *60*, 1107-1114.

[55] M. Fischer, J. Georges, *Chem. Phys. Lett*. **1996**, *260*, 115-118.

[56] R. S. Knox, H. van Amerongen, *J. Phys. Chem. B* **2002**, *106*, 5289-5293.

[57] R. C. Clark, J. S. Reid, *Acta Crystallogr., Sect. A: Found. Crystallogr*. **1995,** *51*, 887-897.

[58] CrysAlisPro, Rigaku Oxford Diffraction, Tokyo, Japan.

[59] G. M. Sheldrick, *Acta Crystallogr., Sect. A: Found. Crystallogr*. **2015,** *71*, 3-8.

[60] G. M. Sheldrick, *Acta Crystallogr., Sect. A: Found. Crystallogr*. **2008,** *64*, 112-122.

[61] O. V. Dolomanov, L. J. Bourhis, R. J. Gildea, J. A. K. Howard, H. Puschmann, *J. Appl. Cryst*. **2009,** *42*, 339-341.

[62] L. Porres, A. Holland, L. O. Palsson, A. P. Monkman, C. Kemp, A. Beeby, *J. Fluoresc*. **2006**, *16*, 267-273.

Entry for the Table of Contents

FULL PAPER

Sterically-crowded BODIPY-based photonic crystals display unusually broad emission profiles while, in liquid solution, the fluorescence yield depends on the number of accreted dipyrrin units.

((Insert TOC Graphic here: max. width: 5.5 cm; max. height: 5.0 cm))

*Özgür Altan Bozdemir, Hatun H. T. Al-Sharif, William McFarlane, Paul G. Waddell, Andrew C. Benniston and Anthony Harriman**

Page No. – Page No.

Solid-State Emission from Mono- and BiChromophoric Boron Dipyrromethene (BODIPY) Derivatives and Comparison with Fluid Solution